Effect of resonant and random excitation on the LHC beam in the context of pulsed hollow electron lens operation.*

Miriam Fitterer,† Giulio Stancari, and Alexander Valishev
Fermi National Accelerator Laboratory, Batavia, Illinois, USA

Stefano Redaelli and Daniel Valuch
CERN, Geneva, Switzerland
(Dated: February 13, 2018)

At the High Luminosity Large Hadron Collider (HL-LHC), a considerable amount of energy is expected to be stored in the beam tails due to the high beam intensity and, in addition, an overpopulation of the tails compared to a Gaussian distribution. To control and clean the tail population, the installation of two hollow electron lenses, one per beam, is presently under consideration. Beside the DC operation of the lenses, also pulsed operation is considered having the advantage to increase the diffusion speed by exerting white or colored noise on the halo particles. For an ideal electron lens, only the halo particles are excited while the core stays untouched. If a residual field is present at the location of the beam core, also the particles in the center are being exposed to noise. In this paper, we present a summary of the LHC experiments conducted in 2016 and 2017 to study the effects on the beam core in case of pulsed operation, where uniform random noise and a resonant excitation were studied. In both cases the excitation was generated with the transverse damper, which is capable of producing almost arbitrary colored noise spectra. In particular the resonant excitation features rich non-linear dynamics inducing unusual changes of the beam distribution and with it emittance and losses. These changes will be one of the main topics of this paper as they have not been observed and studied before in this detail. In addition to the presentation of the experimental and supportive simulation results, we also give first estimates of the residual field at the proton beam core expected from the HL-LHC hollow electron lens for comparison to the noise tolerances obtained in the experiments.

I. INTRODUCTION

Considering past, current and future high energy and intensity colliders, each new machine has represented a considerable leap in stored beam energy with rising values for future accelerators and colliders (see Table I). Recent measurements at the LHC furthermore show that the tails of the transverse beam distribution are overpopulated compared to a Gaussian distribution resulting in a considerable amount of energy being stored in the beam tails alone. In case of the LHC explicitly around 5% of the beam population is stored in the tails above 3.5 σ compared to 0.22% in case of a Gaussian distribution leading to 19 MJ of stored energy in the tails in case of nominal LHC parameters and 34 MJ in case of HL-LHC [6]. This leads to the conclusion that a mechanism is needed to deplete the beam tails in a controlled manner [7].

The most obvious idea is to decrease the collimator gaps or scrape the tails with a collimator type device. This approach is however not feasible as it would generate unacceptably large loss spikes due to the high intensity halo population in the LHC. Most promising are methods, which increase the diffusion speed in the region of the halo particles resulting in a smooth and continuous removal of the high amplitude tails while leaving the core of the beam unperturbed. The diffusing halo particles are then intercepted by the collimation system and removed. This concept is also referred to as active halo control compared to a passive system, which only intercepts the halo particles without actively controlling the diffusion speed (see Fig. 1 for illustration).

In a recent review, the need for such an active halo control system for HL-LHC has been assessed with the conclusion that it would considerably increase the margin and reduce the risk for machine protection compared to the current LHC collimation system being a passive halo control system [7]. In view of the need of active halo control for HL-LHC and for future high power accelerators like HE-LHC and FCC-hh [8, 9], different active halo control methods have been studied in recent years [10], of which the hollow electron lens (HEL) is considered the superior device for the HL-LHC [7]. The beneficial effect of a future HEL for HL-LHC in terms of machine protection and beam collimation can not be, however, deployed at the expenses of the beam core as latter would ultimately lead to a degradation of the performance due to increased particle losses and emittance growth. In this paper, we will concentrate on the assessment in simulations and measurements of possible detrimental effets on the beam core. We will summarize possible sources of perturbations of the proton beam core focusing in par-

* Fermilab is operated by Fermi Research Alliance, LLC under Contract No. DE-AC02-07CH11359 with the United States Department of Energy. This work was partially supported by the US DOE LHC Accelerator Research Program (LARP) and by the European FP7 HiLumi LHC Design Study, Grant Agreement 284404.
† mfittere@fnal.gov

TABLE I. Stored beam energy for different past, present and future colliders. Each new machine represents a leap in stored beam energy.

Collider	Tevatron (protons) [1]	LHC 2016 [2]	LHC nominal [3]	HL-LHC [4]	FCC [5]
Beam energy [TeV]	0.98	6.5	7.0	7.0	50.0
Number of bunches	36	2220	2808	2748	?
Number of particles per bunch	2.90×10^{11}	1.15×10^{11}	1.15×10^{11}	2.2×10^{11}	1.0×10^{11}
Stored beam energy [MJ]	1.6	265.9	362.2	678.0	8400

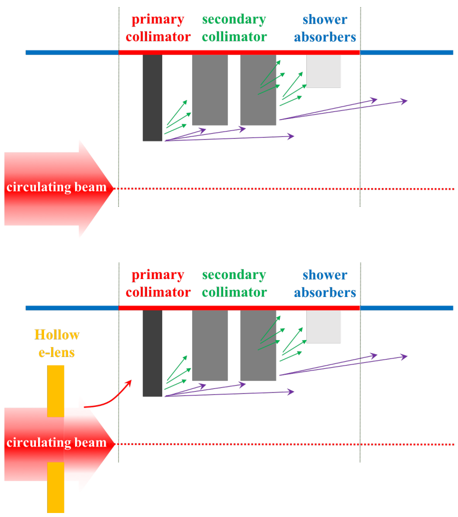

FIG. 1. Sketch of passive halo control as with the collimation system (top) and active halo control using in addition for example a hollow electron lens (HEL) to control the diffusion speed in the region tail region without affected the beam core (bottom).

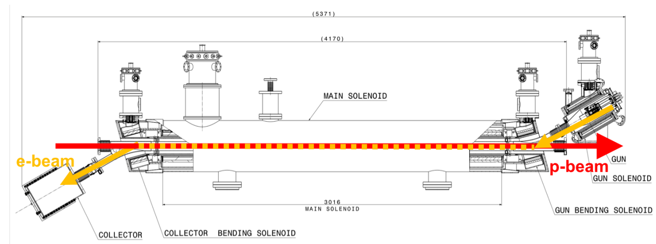

FIG. 2. Layout of HL-LHC HEL. Courtesy of CERN EN-MME group.

ticular on the case of pulsed operation and the beam experiments at the LHC conducted in this context.

This paper is structured as follows: Section II gives an introduction to the concept of HELs and summarizes the design parameters of the HL-LHC HELs. Section III is dedicated to describing the sources of a residual field from the HEL in the core region. Section IV then describes in detail the two beam experiments conducted at the LHC studying the effect of pulsed operation on the proton beam core.

II. HOLLOW ELECTRON LENS FOR HL-LHC

A. General Overview

Electron lenses produce DC or pulsed low energy electron beams, where the electron beam is generated in an electron gun, then guided and confined along a straight section by strong solenoids and finally dumped onto a collector. As an example the conceptual design of the HL-LHC HEL is shown in Fig. 2.

The circulating beam, in case of the LHC the proton beam, is then affected by the electromagnetic field of the electron beam. For the application of active halo control, the electron beam needs to generate an electromagnetic field at the location of the halo particles while leaving the core unperturbed. This field distribution can be achieved by using a uniform hollow distribution in radius $r = \sqrt{x^2 + y^2}$ with inner radius R_1 and outer radius R_2. In this case, the circulating proton beam experiences a radial kick $\theta(r)$

$$\theta(r) = \frac{f(r)}{(r/R_2)} \cdot \theta_{\max}, \tag{1}$$

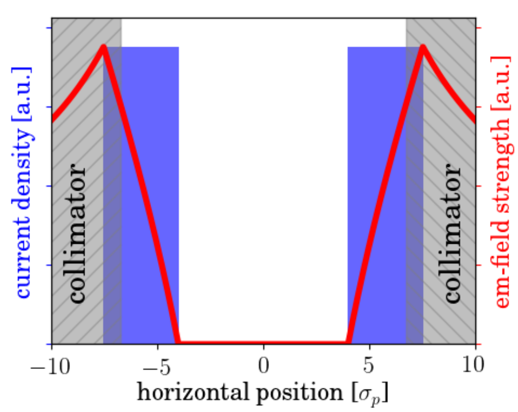

FIG. 3. Illustration of the hollow electron beam distribution (blue), the kick experienced by the proton beam (red) and the collimators (gray).

TABLE II. HL-LHC design parameters at top energy [4] and parameters relevant in connection with the HEL. Optics parameters at HEL are based on a position of the HEL of −40 m for Beam 1 (B1) and +40 m for Beam 2 (B2) from IP4 using HL-LHC optics V1.3 with $\beta^* = 0.15$ m [11].

Beam parameters	Value(B1)	Value(B2)	Unit
Beam energy E_p	7		TeV
Number of bunches n_b	2748		-
Number of particles per bunch N_b	2.2×10^{11}		-
Normalized emittance $\epsilon_{N,x/y}$	2.5		μm
Bunch spacing	25		ns
Optics paramters at HEL (Beam 1) [a]			
β_x at HEL	197.5	280.6	m
β_y at HEL	211.9	262.6 m	
Dispersion D_x at HEL	0.0	0.0	m
Dispersion D_y at HEL	0.0	0.0	m
Proton beam size $\sigma_{p,x}$ at HEL	0.26	0.31	mm
Proton beam size $\sigma_{p,y}$ at HEL	0.27	0.30	mm
scraping position $\sigma_p = \max(\sigma_{p,x}, \sigma_{p,y})$	0.27	0.31	mm

[a] As the Twiss parameters at IP4 do not change during the entire squeeze, and IP4 and the HEL are only separated by a drift space, the Twiss parameters stay constant also at the HEL during the entire squeeze.

where $f(r)$ is a shape function with

$$f(r) = \begin{cases} 0 & , \quad r < R_1, \\ \frac{r^2 - R_1^2}{R_2^2 - R_1^2} & , \quad R_1 \leq r < R_2, \\ 1 & , \quad R_2 \leq r \end{cases} \tag{2}$$

and $\theta_{\max} = \theta(R_2)$ is the maximum kick angle given by

$$\theta_{\max} = \theta(R_2) = \frac{2LI_T(1 \pm \beta_e\beta_p)}{4\pi\epsilon_0 \cdot \left(\frac{p_0}{q}\right)_p \cdot \beta_e\beta_p c^2} \cdot \frac{1}{R_2}, \tag{3}$$

with L the length of the HEL, I_T the total electron beam current, β_e and β_p the relativistic β of electron and proton beam, $\frac{q}{p_0} = (B\rho)_p$ the magnetic rigidity for the proton beam reference particle, c the speed of light and ϵ_0 the vacuum permittivity. The distribution together with the resulting kick are illustrated in Fig. 3. The ±-sign in Eq. 3 represents the two cases of the electron beam traveling in the direction of the proton beam ($v_e v_p > 0$) leading to "−" or in the opposite direction ($v_e v_p < 0$) leading to "+". For hollow electron beam collimation, the beams are chosen to counterrotate. Assuming HL-LHC and HEL design parameters (see Table II–III) the maximum kick of the HEL is:

$$\theta_{\max,\mathrm{B1}} = 392 \text{ nrad} \tag{4}$$

for an inner radius of $R_1 = 4\sigma_p$, outer radius $R_2 = 7.5\sigma_p$, peak current of I_e =5.0 A and Beam 1 of the LHC. Similar values are obtained for Beam 2.

TABLE III. HL-LHC hollow electron lens parameters as in [12].

Geometry	Value	Unit
Length L	3	m
Desired range of scraping positions	3.5-9.5	σ_p
Magnetic fields		
Gun solenoid, B_g	0.2-0.4	T
Main solenoid, B_m	2-6	T
Collector solenoid, B_c	0.2-0.4	T
Compression factor ($k = \sqrt{B_m/B_g}$)	2.2-5.5	-
Electron gun		
Peak yield I_e at 10 keV	5.0	A
Gun perveance P	5	μperv
Inner/outer cathode radius, R_1/R_2	6.75/12.7	mm
High voltage modulator		
Cathode-anode voltage	10.0	kV
Rise time (10%-90%)	200	ns
Repetition rate	35	kHz

B. Operation modes and effects on the beam core

For the HEL two modes of operation are currently under consideration, the DC mode as standard operation mode and the pulsed mode. The main benefit of pulsed HEL operation is the increase in halo removal rates which might become essential as in ideal operation conditions featuring low non-linearities, in particular low chromaticity and octupole current, the DC mode is not effective [13, 14]. For this purpose, two different pulsing patterns are thus considered for the HL-LHC:

- **random excitation:** The electron gun voltage is modulated between:

$$U_{\mathrm{e-gun}} = a \cdot U_{\max} \tag{5}$$
$$+(1-a) \cdot \mathrm{ran}(0,1) \cdot U_{\max} \tag{6}$$

  with $U_{\max}$ the maximum voltage in DC operation, a the modulation strength with $a \in [0,1]$, and $\mathrm{ran}(0,1)$ a uniformly distributed random number between [0,1].

- **resonant excitation:** The HEL is switched on only every k^{th} turn. The excitation can then be represented by:

$$f(t) = \sum_{n=-\infty}^{+\infty} \delta(t - n \cdot (kT)), \tag{7}$$

  where n is the turn number and T the revolution time, and its Fourier series by:

$$f(t) = \text{Ш}_{kT}(t) = \frac{1}{kT} \sum_{n=-\infty}^{+\infty} e^{2\pi i f_n t} \tag{8}$$

$$\text{with } f_n = \frac{n}{k} f_{\mathrm{rev}}, \tag{9}$$

where III_{kT} is the Dirac comb. As can be seen from the Fourier series, k^{th} turn pulsing in general drives k^{th} order resonances [15]. Historically, the k^{th} turn pulsing was used in regular operation in the Tevatron for abort cleaning [16].

As depicted in Fig. 3 and in evidence from Eqs. 1–2, the field at the beam core vanishes in case of an ideal HEL. Effects on the beam core thus only arise from imperfections, where possible sources are the bends of the HEL (see Section III A), as here the electron beam crosses directly the proton beam, and distortions in the electron beam profile (see Section III B). Both sources result in non-linear kicks [17, 18]. In DC operation, these non-linear kicks stay in the shadow of the non-linearities otherwise present in the machine if the electron beam is kept at a decent quality. Tolerances on imperfections are therefore not particularly stringent and of no concern. The picture changes significantly in case of pulsed operation, in which case the electron gun voltage is modulated using a white or colored noise spectrum. If the electromagnetic field of the HEL does not vanish at the proton beam core, noise is transferred not only to the halo particles, as intended, but also to the beam core. Tolerances on the residual field in this case rapidly become much more stringent than in the case of DC operation. Studies of the effect of the HEL on the beam core therefore focus on this mode of operation which will also be the main subject of this paper.

III. SOURCES OF RESIDUAL FIELD IN THE PROTON BEAM CORE REGION AND FIRST ORDER ESTIMATES

With the current HEL layout as shown in Fig. 2, parasitic kicks on the proton beam core can arise in the central region due to profile imperfections in the electron beam and at the entrance and exit of the HEL, where electron and proton beam overlap. Currently, no HEL is installed in the LHC, and the kick on the proton beam core must therefore be emulated with the help of other devices already installed in the LHC. For this purpose the kick is approximated to first order by a dipole kick. During the experiments presented in this paper, the dipole kick with the corresponding excitation pattern could then be applied with the LHC transverse damper as will be described in detail in Section IV B. As will be shown in Sec. III A and III B, the expected kick to first order from the HEL bends is estimated to be (Eq. 14):

$$\Delta x'_{\text{bends}}, \Delta y'_{\text{bends}} \approx 0.5\,\text{nrad}, \tag{10}$$

and for the central region due to profile imperfections (Eq. 16):

$$\Delta x'_{\text{central region}}, \Delta y'_{\text{central region}} \approx 19.6\,\text{nrad} \tag{11}$$

where the current HEL design parameters are used (see Table II–III). The contribution from the central region is clearly dominating.

A. Uncompensated kicks from HEL bends

As reference for the estimate of the dipole component originating from the HEL bends, the symplectic map derived in [17] is used. In this case the HEL bends are modeled as a bent cylindrical pipe with a static charge distribution of 1 A and 5 keV electrons deflected in the horizontal plane, where the parameters were her still based on the old gun design for the Tevatron electron lens Giulio, is this correct?. In case of an U-shaped HEL, the transverse dipole kicks at entrance and exit add up, while for a S-shape the kicks compensate each other. For this reason a S-shape has been chosen for the HL-LHC HEL (see Fig. 2). Assuming and S-shaped HEL, uncompensated kicks therefore only arise from imperfections, which can originate from profile imperfections and current fluctuations. As a first estimate, we assume in this paper 10% fluctuations between the entrance and exit and, in addition, that the kicks from entrance and exit due to these imperfections add up. Using the electric field calculations in [17], the maximum values for the integrated electric field are then

$$\int_{z_1}^{z_2} E_{x,y} dz = 10\ \text{kV}. \tag{12}$$

Neglecting magnetic effects and scaling to HL-LHC and HEL design parameters (Tables II–III) yields a kick of [15]:

$$\int_{z_1}^{z_2} E_y dz = 36\ \text{kV} \Rightarrow \Delta y' = 5.1\ \text{nrad} \tag{13}$$

Assuming now 10% fluctuation between entrance and exit kick, the expected kick from the HEL bends is

$$\Delta x', \Delta y' \approx 0.5\ \text{nrad}. \tag{14}$$

B. Kicks in the central region (main solenoid)

For a perfectly annular and axially symmetric profile, the field in the region of the proton beam core vanishes as can be seen from Eq. 2 and as illustrated in Fig. 3. Fields at the location of the proton beam core thus only arise in case of profile imperfections of the electron beam, in particular if the axial symmetry is broken. Recently, the latest LHC hollow electron gun prototype was characterized at the Fermilab electron lens test stand [21]. A typical measurement of the electron beam current density is shown in Fig. 4. As at the test stand the solenoidal fields required for the HL-LHC electron lens can not be reached, an estimate of the electron beam profile for HL-LHC can only be obtained through simulations. For this purpose, the measured distribution is compressed to the inner electron beam radius of 0.97 mm. Afterwards an input distribution with 40 000 particles is generated. As boundary condition, the LHC inner beam pipe radius

TABLE IV. Beam parameters and machine configuration as used in the two resonant excitation experiments in 2016 and 2017 [19, 20]. The plane of the excitation is abbreviated with H for horizontal, V for vertical and H+V horizontal and vertical at the same time.

Parameter	Experiment 2016	Experiment 2017
beam	Beam 1	
beam energy	injection energy, 450 GeV	
single bunch intensity	0.7×10^{11}	
normalized emittance	$2.5 - 3.5\ \mu$m	
4σ bunch length	1.3 ns	
1σ bunch length	9.7 cm	
number of bunches	$12 \times 4 = 48$ single bunches	$3 \times 72 = 216$ bunches (+ 1 pilot + 12 nominal)
injection optics, $\beta^* = 11$ m	standard optics 2016	standard optics 2017
Landau damping octupoles	$I_{\mathrm{MO}} = +19.6$ A for MOF circuit and $I_{\mathrm{MO}} = -19.6$ A for MOD circuit (standard 2016 settings)	
working point (Q_x, Q_y)	(64.28,59.31)	(62.27,60.295)
chromaticity (Q'_x, Q'_y)	(+15,+15)	
pulsing patterns	7^{th} turn H; 10^{th} turn V;	7^{th} turn H,V,H+V; 8^{th} turn H,V,H+V; random H,V,H+V;

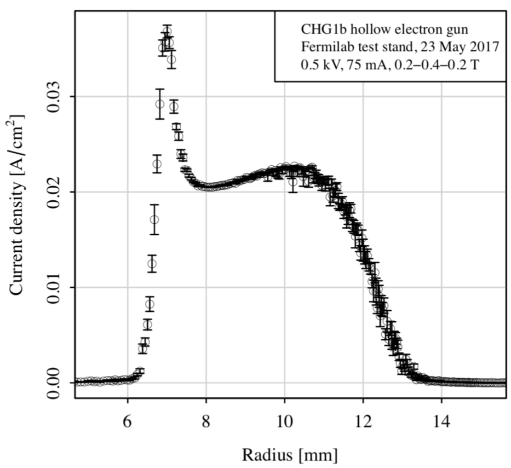

FIG. 4. Current density from measurements of the CHG1b hollow electron gun at the Fermilab electron lens test stand in 2017 [22]. Replace by 2D simulations - Giulio.

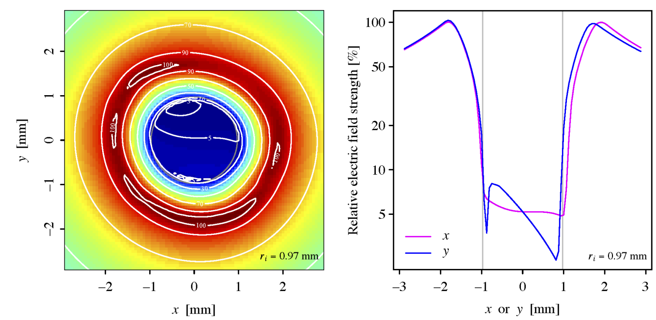

FIG. 5. Calculated relative electric field for the new CHG1b hollow electron gun in the x-y plane (left) and as 1-dimensional cuts though the x- and y-axes (right). The field calculations are based on measurements at the Fermilab test stand combined with WARP calculations of the electric potentials and fields in a cylindrical beam pipe.

$b = 30$ mm is used. The potential and fields can then be calculated with the particle in cell simulation code WARP [23] yielding the relative electric field strengths shown in Fig. 5. The electric field can in general be scaled with the beam current and energy, but can not easily be scaled with the inner and outer radius of the electron beam distribution. Therefore it is essential to track a distribution with the correct dimensions. Further details on the measurements and WARP simulations can be found in [22].

Using these measurements and calculations of the relative electric field strengths in the transverse plane (Fig. 5), we obtain an average field in the hole of

$$E_{\mathrm{rel}} = 5\% \tag{15}$$

For a maximum kick of 392 nrad as derived in Eq. 4, the estimated dipole kick amplitude at the proton beam core then is:

$$\Delta x'_{\mathrm{central\ region}}, \Delta y'_{\mathrm{central\ region}} = 19.6\,\mathrm{nrad} \tag{16}$$

IV. EXPERIMENTAL AND SIMULATION SETUP

A. Overview of LHC experiments

The experiments at the LHC which are presented in this paper were aiming at deriving tolerances on the residual HEL field at the location of the beam core in case of pulsed operation. In total, two experiments were conducted, the first one in 2016 [19] and the second one in

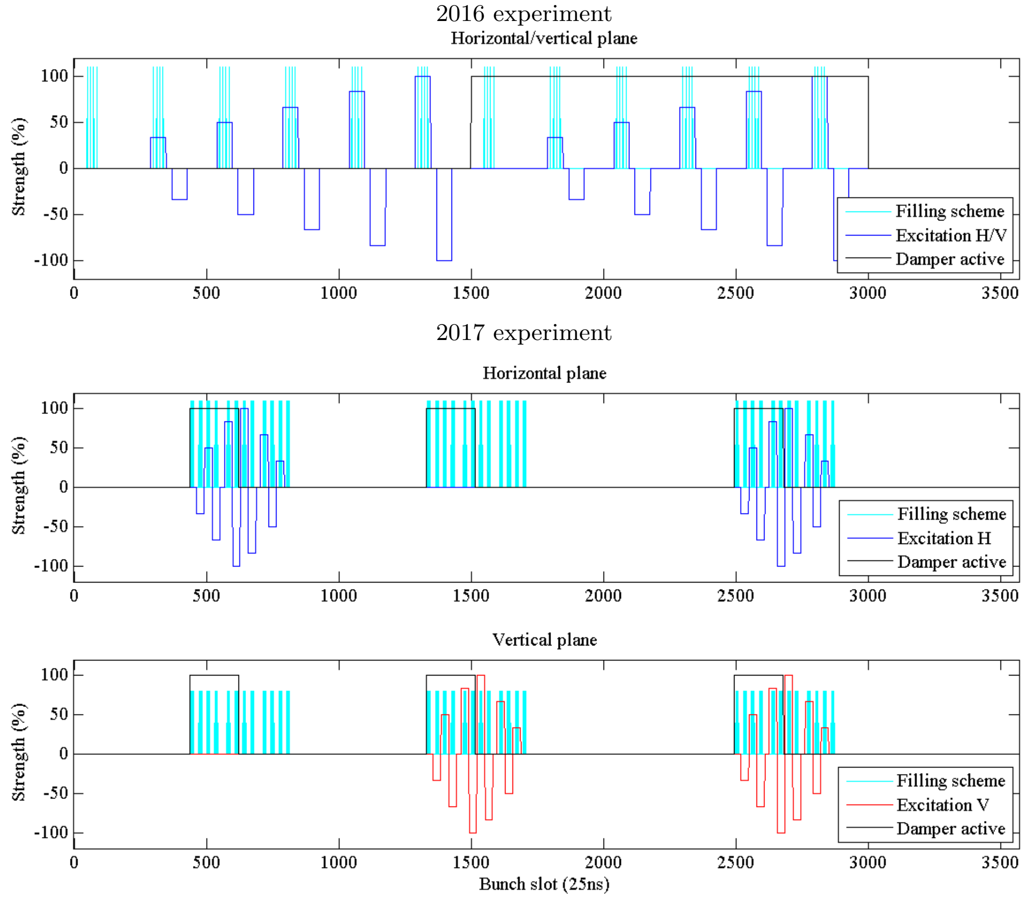

FIG. 6. Filling and excitation scheme for LHC experiments in 2016 (top) and 2017 (bottom). In 2016 the same excitation amplitude was applied on a group of 4 bunch while in 2016 the number was increased to 6 bunches. In 2016 the excitation was also only applied in one plane leading to $2 \times 24 = 48$ bunches in total in 2016 and $3 \times 2 \times 36 = 216$ bunches in 2017.

2017 [20]. Beam and machine parameters for both experiments are summarized in Table IV. Preceding the beam experiments, simulations were performed to identify the most effective k^{th} turn pulsing pattern and yield estimates for losses and emittance growth. The two k^{th} turn pulsing patterns with the largest effect, one k^{th} turn pulsing pattern with no effect and the random excitation could then be experimentally tested in the LHC. In order to test the reproducibility of the results at least on the example of one pulsing pattern, the 7^{th} turn pulsing was first tried in 2016 and then repeated in 2017.

During the experiments the losses were measured with the fast beam current transformers (FBCTs) and the emittance and transverse beam profiles with the beam synchrotron radiation telescope (BSRT), where all instruments are capable of delivering bunch-by-bunch data. The analysis of the BSRT profiles is quite involved and we will therefore focus in this paper only on the direct comparison of the profiles. A detailed description of the analysis with more details can be found in [24] and for the individual experiments in [19, 20].

B. Excitation with transverse damper and filling scheme

The primary function of the transverse feedback system in LHC, also referenced to as ADT, is to provide injection oscillation damping and actively damp the coupled bunch instabilities driven by the machine impedance. The main building blocks of the ADT system are stipline pickups at the position Q7 and Q9 at Point 4 of the LHC, connected to the beam position measurement modules at the surface, the digital signal processing modules (mDSPU) and a set of tetrode power amplifiers feeding electrostatic kickers in the RF zone of the LHC [25, 26]. Though originally designed to damp the undesired transverse activities only, the damper is being routinely used for sophisticated beam excitations as well thanks to the state of the art digital signal processing hardware. These include among others abort and injection gap cleaning, single bunch excitation for tune and linear coupling measurements and special modes of operation for dedicated experiments at the LHC.

The transverse feedback is in general active during the whole LHC cycle, therefore it is critical that the noise introduced by the system does not contribute to any emittance growth. The typical machine cycle requires a short damping time of 10-20 turns (high feedback gain) for injection oscillation damping, which is increased during the ramp and collisions to 50-100 turns (lower feedback gain). It has been demonstrated that noise introduced by the transverse feedback system itself is sufficiently low not to introduce any measurable emittance growth [27]. All excitation signals referenced to in this paper are digitally synthesized in the damper's digital signal processing units and therefore can be considered as "noise-free". This point is important as then the effect on the beam can be attributed entirely to the applied excitation and any effect due to unwanted residual noise can be neglected.

The resonant excitation experiment in 2017 involved simultaneous measurements on three groups of 72 bunches with a dedicated excitation pattern and transverse feedback configuration on each sub-group of 6 bunches. In 2016 a similar configuration was used, but with only 48 bunches in total and sub-groups of 4 bunches. Both schemes are illustrated in Fig. 6. In order to reduce the error of the measurements, the observables are averaged over each sub-group of bunches experiencing the same excitation amplitude, yielding in total 5 different amplitudes $n\Delta A$ with $n = 1, \cdots, 5$ plus the references bunch without excitation for each transverse feedback configuration and excitation plane. Furthermore, the experiments were usually split in 3 different parts:

Part 1: No excitation is applied in order to allow the distribution to reach an equilibrium state after injection.

Part 2: The excitation is applied with a first maximum excitation amplitude of $A_{\max,1} = 5\Delta A_1$.

Part 3: The maximum excitation amplitude is further increased to $A_{\max,1} < A_{\max,2} = 5\Delta A_2$.

Each part lasted approximately 10-15 minutes, which is considered to be a long enough time window to allow the beam distribution to reach its new equilibrium state. In the plots of the experimental results shown later in the paper, the maximum excitation amplitude is indicated with black horizontal arrows, while the average of each sub-group of bunches with the same excitation amplitude $n\Delta A$ is distinguished with different colors.

The excitation in the horizontal and the vertical plane is generated by a different set of signal processing hardware, however during this experiment the signals were synchronized at a turn level. This means the bunches of the third group (of 72 bunches) experienced the kick in both horizontal and vertical plane during the same turn.

The ADT kicker deflection angle is calculated from the kicker geometry and the excitation voltage on the deflection plates. The excitation voltage used in the experiments is a complicated waveform, generated by a very complex hardware (digital signal processor, chain of transmission lines, low and high power amplifiers). The peak excitation voltage (and subsequently the kick) seen by the beam can be only indirectly measured using the probes on each kicker. The measured values are therefore believed to be known with an error margin of 10-15% for the experiments in 2017 and 50% in 2016. The error in 2016 is much larger as no calibration of the ADT was performed beforehand, which was done in 2017. The maximum kick strength reachable with the ADT at injection without risking saturation is 96 nrad. As an example Fig. 7 shows the oscillation amplitude of each bunch in both H and V planes captured by the LHC real time transverse activity monitor during the 2017 experiments and an excitation with 8$^{\text{th}}$ turn pulsing. The measured activity is well in line with the expected excitation pattern.

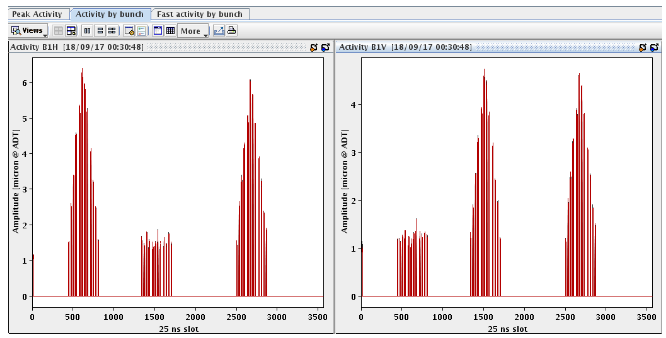

FIG. 7. Bunch by bunch excitation detected by the real time transverse activity monitor during the 2017 experiment and an excitation with 8th turn pulsing.

C. Overview of simulations

For the preparation and interpretation of the experiments two different types of simulations were performed:

1. tracking of a Gaussian distribution, referred to as "distribution tracking" in this paper, to obtain loss rates and emittance growth,

2. Frequency map analysis (FMA) for the visualization of resonances [28].

For both simulation types, the tracking code Lifetrac [29] was used. The simulation parameters are summarized in Table V. Further details on the simulations are given in Refs. [15, 20].

V. EXPERIMENTAL AND SIMULATION RESULTS

In the following we will jump forth and back between both experimental and simulation results as the experimental results are best understood on the base of the simulations. In summary, the most efficient pulsing patterns could be successfully predicted in simulations, which we

TABLE V. Summary of simulation parameters for the distribution tracking and FMA analysis. For details see [15, 20].

Parameter	distribution tracking	FMA
beam	Beam 1	
beam energy	450 GeV	
emittance	3.5 μm	2.5 μm
4σ bunch length	1.3 ns	
1σ bunch length	9.7 cm	
particle distribution	6D Gaussian distribution (10^4 particles)	equally spaced grid in x, y up to 10 σ with $\frac{\Delta p}{p_0} = 0$
turns tracked	10^6 turns	10^4 turns
optics	2016 or 2017 injection optics, $\beta^*_{\mathrm{IP1/5}} = 11$ m	
machine imperfections	standard errors with $a_1 = b_1 = 0$[a]	no errors
octupoles	$I_{\mathrm{MOF}} = +19.6$ A, $I_{\mathrm{MOD}} = -19.6$ A	
tune (Q_x, Q_y)	(64.28,59.31) for 2016, (62.27,60.295) for 2017	
chromaticity (Q'_x, Q'_y)	(+15,+15)	
transv. aperture	5.7 σ	-
long. aperture	10 σ	-

[a] Orbit errors are disabled due to different implementation of the a_1, b_1 errors in Lifetrac and MAD-X. b_2 errors are adjusted to yield an average (over 60 seeds) peak β-beat of 15% as expected from optics measurements in the LHC.

will demonstrate on the example of the 2016 experiments (see Sec. V A). Afterwards we will present the simulation and experimental results of the tested excitation patterns, explicitly the 10$^{\text{th}}$ turn, 7$^{\text{th}}$ turn and 8$^{\text{th}}$ turn pulsing in Secs. V B–V D as well as the random excitation in Sec. V E. As a last chapter, Sec. V F, we will address the influence of the transverse damper in the presence of an external excitation source on emittance, losses and beam distribution.

Quantitative predictions of loss rates and emittance growth proved in general challenging as both observables are influenced in addition by the natural noise present in the LHC, originating for example from vibrations and magnetic field ripple. The observed effect is then the result of the interaction of the external excitation with the natural noise. At injection, this natural noise component is not known and thus presents a very influential but undefined input to the simulations. Beside the natural noise, also collective effects like intra-beam scattering and electron cloud influence the time evolution of emittance and losses. Both are also not taken into account in these simulations, but the effect was minimized during the experiments by choosing an as small as possible bunch intensity of only 0.7×10^{11} protons per bunch.

A. Dependence on the pulsing pattern

The effect of each pulsing pattern in comparison to the other patterns can be identified by the means of the loss rate and emittance growth from the distribution tracking. As an example, the simulation results for the 2016 experiment are shown in Fig. 8 featuring a clear dependence of both parameters on the pattern.

The largest losses are observed for 3$^{\text{rd}}$, 7$^{\text{th}}$ and 10$^{\text{th}}$ turn pulsing and a uniform random excitation. As the bunch length decreases in accordance with the losses, the losses can be mostly associated to off-momentum particles hitting the transverse aperture. Only 7$^{\text{th}}$ and 10$^{\text{th}}$ turn pulsing as well as random excitation exhibit considerable emittance growth. Compared to any resonant excitation, the random excitation has by far the strongest effect.

The sensitivity to 7$^{\text{th}}$ and 10$^{\text{th}}$ turn pulsing is also observed in absence of machine errors in which case the only source of non-linearities are sextupoles and octupoles [15] suggesting that latter are responsible for the observed sensitivity. The driven resonances are revealed by the FMA analysis shown in Fig. 9. The $7Q_x$ resonance is excited in case of the 7$^{\text{th}}$ turn pulsing and the $10Q_x$ and $10Q_y$ resonance in case of the 10$^{\text{th}}$ turn pulsing. As octupoles can only drive even resonances, the source of the $7Q_x$ resonances are the sextupoles while the octupoles only generate the tune footprint. The other pulsing patterns do not exhibit any increase in losses or emittance growth without magnetic errors and their effect can be thus attributed to the magnetic field errors, implying also the seed chosen for the simulation.

One may have noticed that the emittance in case of the 7$^{\text{th}}$ and 10$^{\text{th}}$ turn pulsing starts at an increased initial value and then stays almost constant during the entire simulation time, which usually points to an error in the chosen simulation setup. This behavior is however typical for any resonant excitation and can be ascribed to the adjustment of the beam distribution during the first 10^4 turns to a new equilibrium. As the beam distribution is only dumped every 10^4 turns, this initial fast adjustment manifests itself in an increased initial emittance value in Fig. 8, and also any other simulations over 10^6 turns presented in this paper. Besides an increased emittance, the new distribution also becomes non-Gaussian. This is illustrated by means of the residual in respect to the Gaussian distribution for 7$^{\text{th}}$ and 10$^{\text{th}}$ turn pulsing in Fig. 10. This initial fast change of the beam distribution is not an artifact of the simulation, but has been, to the knowledge of the authors, also for the first time experimentally observed during the 2016 and 2017 LHC experiments presented in this paper. The timescale of this fast adjustment is in experiments however much slower than predicted in simulations — on the timescale of minutes compared to seconds.

In the presence of only a resonant excitation, this modified distribution is stable in simulations with a constant emittance. As we will see later, an increase of the emittance with the applied excitation amplitude is however observed experimentally not matching the prediction by simulations. By adding a random noise component representative for the natural noise present in the LHC, the constant emittance is changed in simulations to an excitation amplitude dependent emittance growth after an initial adjustment phase. In case of random uniform noise, the excitation leads to constant emittance growth without any initial adjustment phase. The interaction with the natural noise source then only results in an underestimation of loss rates and emittance growth as it is basically equivalent to the application of random noise with an increased amplitude. In addition to the experiments presented in this paper, the effect of a random excitation was also studied in a separate experiment at the LHC for the case of colliding beams [30, 31].

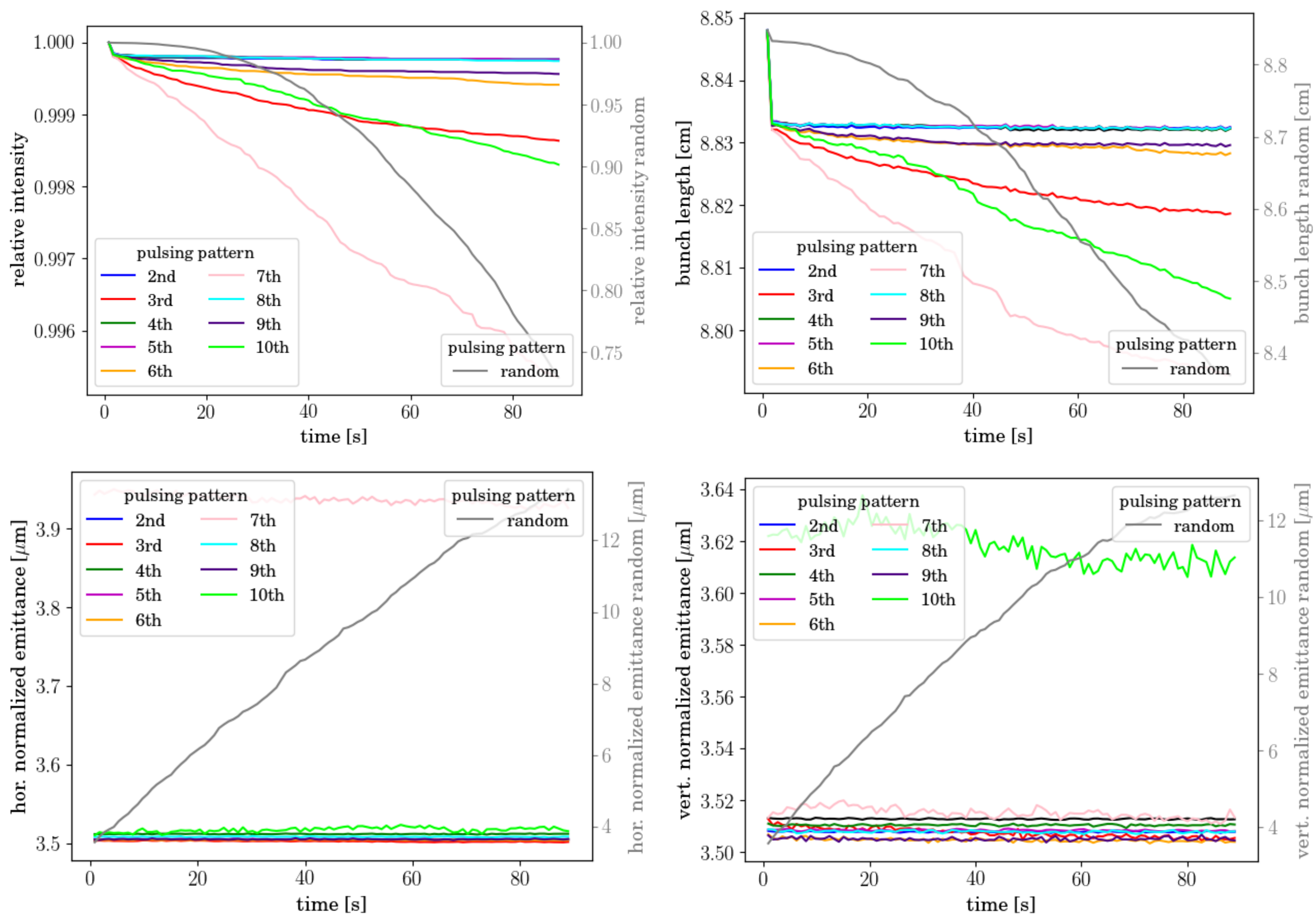

FIG. 8. Relative intensity (top left), bunch length (top right) and horizontal (bottom left) and vertical (bottom right) emittance for different pulsing patterns obtained from distribution tracking based on the 2016 injection optics with $(Q_x, Q_y) = (64.28, 59.31)$ with standard errors. The resonant and random excitation respectively is applied in both planes with an amplitude of 96 nrad. No random noise component is added in addition.

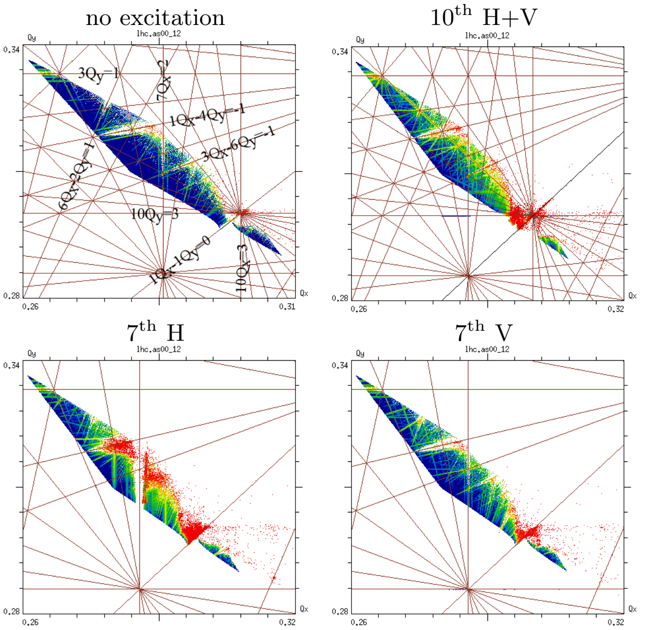

FIG. 9. FMA analysis without excitation (top left) for 10^{th} turn pulsing in H+V (top left) and for 7^{th} pulsing only in H (bottom left) and only in V (bottom right) and based on the 2016 injection optics with no machine errors and a tune of (64.28,59.31). The excitation is 120 nrad in the corresponding plane. The absence of a strong excitation of any resonance in case of 7^{th} turn pulsing only in V and the strong excitation in case of pulsing only in H confirms the excitation of the $7Q_x$ resonance. For 10^{th} turn pulsing there is in contrast no significant difference between pulsing only in H, only in V or in H+V (see Appendix A, Fig. 28).

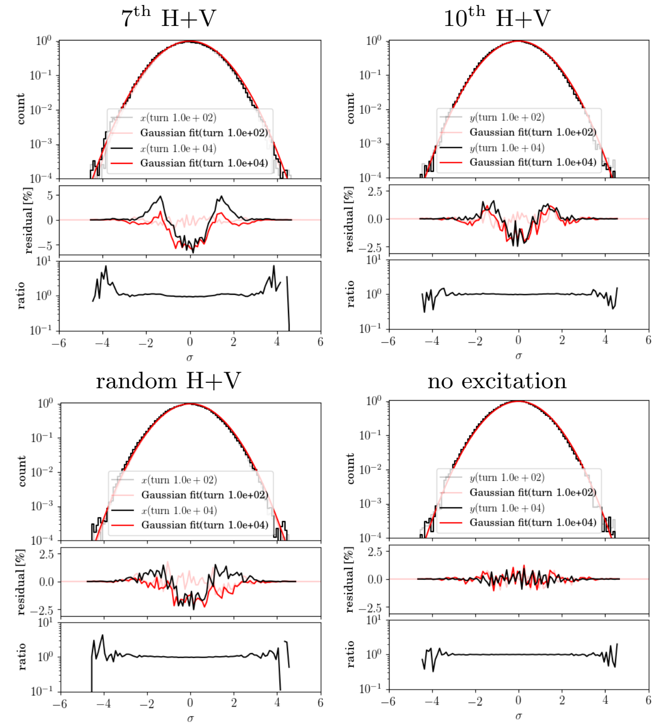

FIG. 10. Horizontal beam distribution for 7^{th} turn pulsing (top left), vertical beam distribution for 10^{th} turn pulsing (top right) and horizontal (bottom left) and vertical (bottom right) beam distribution for random excitation from distribution tracking simulations based on the 2016 injection optics with $(Q_x, Q_y) = (64.28, 59.31)$ and standard errors. The excitation is applied in both planes with an amplitude of 96 nrad. The residual is defined as the final distribution (here after 10^4 turns) minus the initial distribution (here after 10^2 turns) as %, and the ratio as the final distribution divided by the initial distribution. The red line in the plot of the residual is the difference between the Gaussian fit of the distribution and the distribution itself.

B. 10^{th} turn pulsing

The 10^{th} turn pulsing pattern was tested in 2016 with an excitation in the vertical plane only. As this was the first time a resonant excitation was tested in the LHC, only in total 48 bunches could be injected in order to still guarantee the protection of the machine. To test different excitation amplitudes during one fill and have enough statistics, the excitation was therefore only applied in one plane. As described earlier, the experiment started with a period of 12 minutes without excitation in order to let the beam distribution fully adjust to its equilibrium state after injection. Afterwards the excitation was applied with the excitation scheme shown in Fig. 6 and a maximum excitation amplitude of $A_{\text{max}} = 5\Delta A = 48$ nrad for a total of 11 minutes. The excitation was then further increased to the maximum value reachable without saturation of $A_{\text{max}} = 5\Delta A = 96$ nrad and kept for 11 minutes. In both cases, the excitation induced the following changes:

1. Increase of the loss rate with the excitation amplitude (Figs. 11.
2. Increase of the emittance growth with the excitation amplitude in the vertical plane but not in the horizontal plane (Fig. 11).
3. Change of the beam distribution for the excited bunches (Fig. 12).

As loss rates, emittance growth and beam distribution stayed unchanged for the 4 reference bunches, the above observations can be also truly associated with the effect of the 10^{th} turn pulsing. These experimentally obtained scalings of the loss rate and emittance growth with the excitation amplitude can be then used for the actual specification of the hollow electron lens.

Besides the numerical determination of tolerances, the vertical emittance actually features indeed the strange and interesting behavior predicted in simulations: a fast adjustment phase of the beam distribution visible as a rapid increase of the emittance followed by the reach of a new equilibrium distribution apparent by a slower continuous emittance growth. These two phases are indicated in Fig. 11 in blue and black.

Thanks to the good performance of the Beam Synchrotron Radiation Telescope (BSRT) [24], the distribution changes indirectly observed as changes of the emittance could also be for the first time directly measured. As example Fig. 12 shows the vertical profile of a reference bunch and one bunch experiencing the maximum excitation of $5 \cdot \Delta A = A_{\text{max}} = 48$ nrad and afterwards 96 nrad. The distribution of the excited bunch not only changes but becomes clearly non-Gaussian, while the reference bunch stays unchanged. The simulation results from the distribution tracking for 10^{th} turn pulsing and without (solid line) and with (dotted line) additional random noise component to emulate the natural noise present in the LHC are shown in Fig. 13. As no estimate of the natural noise is available at injection for the LHC, a first estimate is obtained by scaling the estimate for 6.5 TeV [30, 31] by the magnetic rigidity to the injection energy of 450 GeV. This yields a maximum kick amplitude at the transverse damper of approximately

$$\theta_{\text{random,ADT,max}}(450 \text{ GeV}) = 6 \text{ nrad}. \tag{17}$$

As can be seen from simulations, adding a random noise component not only yields the correct qualitative behavior of the emittance but also increases the losses. As the losses are in general underestimated in simulations compared to the experimental results, the discrepancy between simulations and experiment can be thus reduced. To better compare the experimental results for the two different maximum excitation amplitudes applied for slightly different time intervals and also the simulations conducted for a much shorter interval of only 90 s, we define the relative loss rate R:

$$R = \frac{I_{\text{start}} - I_{\text{end}}}{I_{\text{start}} \cdot \Delta t} \tag{18}$$

where I is the intensity and Δt the time interval during which the excitation with fixed A_{max} is applied during the experiments or the duration of the simulation respectively. A qualitative comparison of the loss rates obtained in experiments and simulations is shown in Fig. 14 featuring a surprisingly good agreement. It should be also kept in mind that the additional random noise component considerably influences the simulation results and as long as it is unknown should be seen more as a fit parameter than a real experimentally confirmed input parameter. The measured loss rates for $A_{\text{max}} = 48$ nrad and $A_{\text{max}} = 96$ nrad should furthermore follow the same scaling. Instead the loss rates for the same excitation amplitude are smaller for $A_{\text{max}} = 96$ nrad compared to $A_{\text{max}} = 48$ nrad. That losses and also emittance growth for a fixed excitation amplitude do not exactly agree for both experiments, is a general tendency observed in all experiments. As the second excitation however starts from an already by the previous excitation changed beam distribution, the difference is however not surprising and can be explained by this difference in initial conditions. For checking the reproducibility of the results in a possible future experiment, it would be interesting to see if the same loss rates are measured if for each A_{max} a new fill is used.

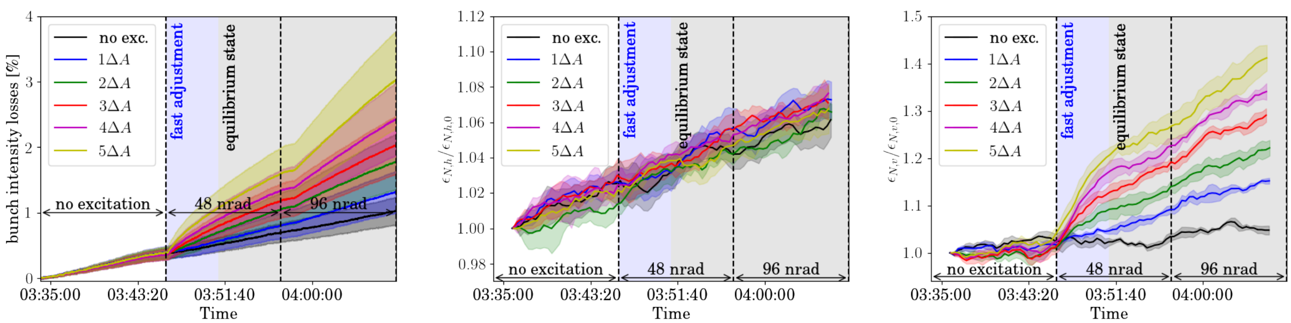

FIG. 11. Relative intensity (top) and relative horizontal (bottom left) and vertical (bottom right) emittance averaged over the bunches experiencing the same excitation amplitude during the 2016 experiments. For all bunches the damper was not active. Relative refers here to the normalization to the initial value. For each maximum amplitude $A_{\max} = 48$ nrad and 96 nrad indicated with black arrows, the excitation amplitude was linearly increased for each group of 4 bunches (see Fig. 6). The different colored solid lines labeled with $n\Delta A$ are the average over the 4 bunches with the same excitation amplitude together with the 1σ standard deviation shown as envelope. The area with a blue background indicates the fast adjustment period of the beam distribution transitioning into a new equilibrium state highlighted with a gray background.

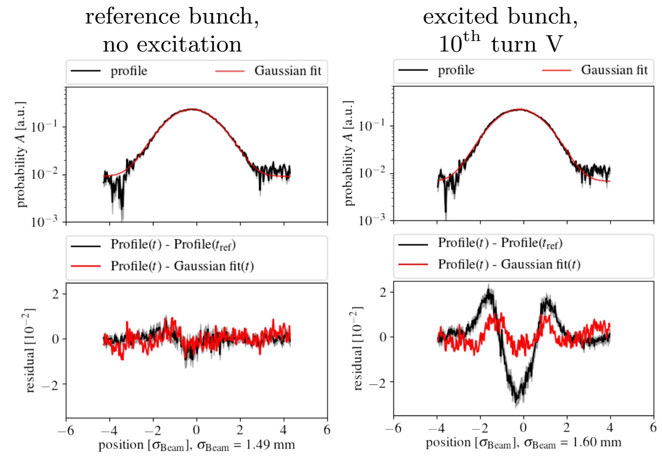

FIG. 12. Vertical beam profiles measured with the Beam Synchrotron Radiation Telescope (BSRT) during the 2016 experiments. The profiles are taken at the end of the 10^{th} turn pulsing in V. For both bunches the transverse damper is not active. The black line in the plot of the residual is the current profile minus the profile before applying the excitation and is a measure for the overall change of the distribution. The red line is the current profile minus its Gaussian fit, which gives and indication for the deviation of the distribution from a Gaussian distribution. For details on the analysis it is referred to [24]. The distribution of the reference bunch (left), here slot 50, stays unchanged, while the bunch experiencing the maximum excitation (right), here slot 1300, clearly shows a change to a non-Gaussian distribution.

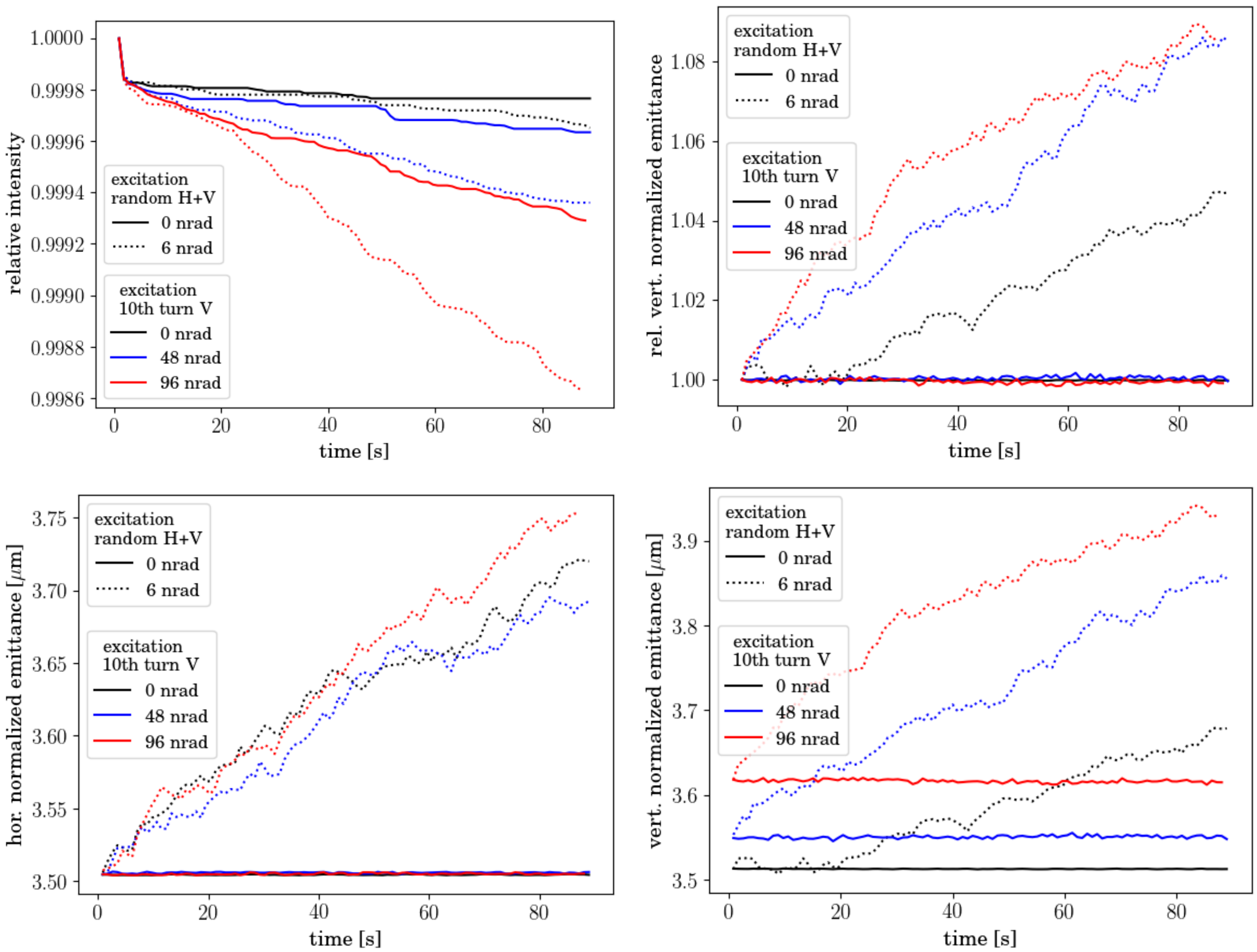

FIG. 13. Relative intensity (top left) and relative vert. emittance (top right), and hor. (bottom left) and vert. (bottom right) emittance obtained from simulations (distribution tracking) based on the 2016 injection optics with standard errors and $(Q_x, Q_y) = (64.28, 59.31)$. The solid line indicates an excitation with only 10^{th} turn pulsing in V and the dotted line with 10^{th} turn pulsing in V plus a random dipole noise component in H+V of 6 nrad.

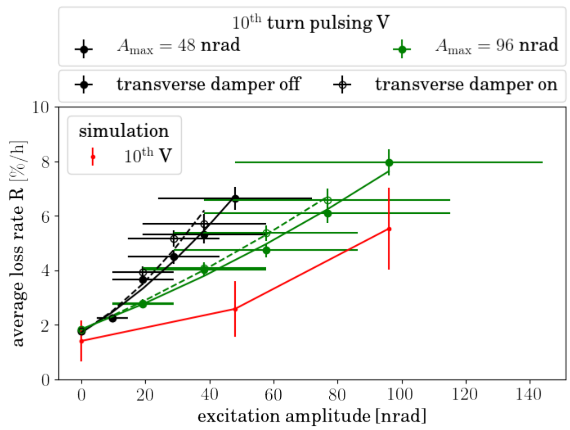

FIG. 14. Comparison of scaling of loss rates R as defined in Eqn. 18 with the excitation amplitude for 10^{th} turn pulsing in V. The experimental results for a maximum excitation of $A_{\max} = 48$ nrad are shown in black and for $A_{\max} = 96$ nrad in green. The excitation amplitude error is 50% and the error on the loss rate is the pure statistical error on the mean. The simulation results (see Fig. 13) for 2016 injection optics, standard errors, $(Q_x, Q_y) = (64.28, 59.31)$, 10^{th} turn pulsing in V plus random dipole noise in H+V of 6 nrad are shown in red together with their statistical error. The loss rates follow approximately a quadratic behavior illustrated by a second order polynomial fit to the data shown as solid (for bunches with transverse damper off) or dashed (for bunches with transverse damper on) line.

C. 7^{th} turn pulsing

The 7^{th} turn pulsing pattern has been tested during both experiments in 2016 and 2017 and was intended to serve as a proof for the reproducibility of the experimental results. Unfortunate for this experiment, the machine tune was changed in standard operation from (64.28,59.31) in 2016 to (62.27,60.295) in 2017 accompanied by a slight change in optics considered irrelevant in the context of the presented measurements. The attempt to change back to the fractional tunes of (.28,.31) as chosen in 2016 lead to large losses during the 2017 experiment and therefore the 2017 working point of (62.27,60.295) had to be used instead. This change in tune entailed a change in the driving resonances, from previously the $7Q_x$ resonances in 2016 (see Fig. 9) to the $7Q_x$, $7Q_y$ and $7Q_x+7Q_y$ resonance in 2017 (see Fig. 15).

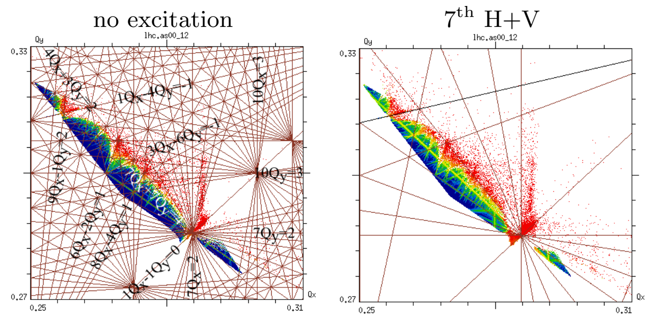

FIG. 15. FMA analysis in frequency space without excitation (left) and for 7^{th} turn pulsing in H+V (right) based on the 2017 injection optics with no machine errors and a tune of (62.27,60.295). The excitation is 96 nrad in both planes. The $7Q_x$ and $7Q_y$ resonance are both excited and in addition the 14th order $7Q_x + 7Q_y$.

Consequently, the effect of the 7^{th} turn pulsing on the beam losses, emittance and beam distribution also differ as depicted by the comparison of the distribution tracking for both experiments in Fig. 16, the qualitative comparison of the experimental results in Table VI, the comparison of the measured emittance in Fig. 17 and loss rate in Fig. 18.

TABLE VI. Overview of the effect of 7^{th} turn pulsing during the two resonant excitation experiments in 2016 [19] and 2017 [20]. The plane of the excitation is abbreviated with H for horizontal, V for vertical and H+V for horizontal and vertical at the same time.

Parameter	Experiment 2017	Experiment 2016
optics	2017 injection optics	2016 injection optics
tune (Q_x, Q_y)	(62.27,60.295)	(64.28,59.31)
excitation plane	H,V and H+V	H
losses	similar loss rates for pulsing in H,V and H+V	large losses for pulsing in H
hor. emit. growth	no	yes, very small
vert. emit. growth	yes, for pulsing in V and H+V	no

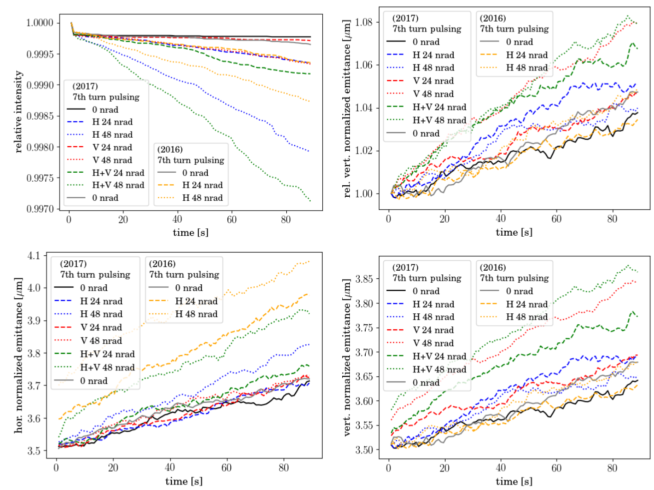

FIG. 16. Relative intensity (top left), relative vertical emittance (top right), and horizontal (bottom left) and vertical (bottom right) emittance obtained from distribution tracking based on the 2016 injection optics with standard errors and $(Q_x, Q_y) = (64.28, 59.31)$ and 2017 injection optics with standard errors and $(Q_x, Q_y) = (62.27, 60.295)$. The solid line indicates an excitation with only a random dipole noise component in H+V of 6 nrad, and the dotted and dashed line the results for 7^{th} turn pulsing with two different excitation amplitudes plus a random dipole noise component in H+V of 6 nrad.

The simulation results from the distribution tracking shown in Fig. 16 in general predict in terms of emittance for the two experiments:

2016 experiment: Excitation amplitude dependent emittance growth in the horizontal but not in the vertical plane.

2017 experiment: Excitation amplitude dependent emittance growth in the vertical plane but not in the horizontal plane for an excitation in V and H+V. For an excitation only in H no emittance growth is observed.

Similar changes of the emittance as predicted in simulations were also experimentally observed as depicted in Fig. 17, where emittance growth was observed only in the horizontal plane for pulsing in H in 2016, and only in the vertical plane for pulsing in V and H+V in 2017 with no emittance growth at all for pulsing in H. Just as for the 10^{th} turn pulsing, the emittance growth can be divided also for the 7^{th} turn pulsing in a phase of fast adjustment of the beam distribution and the reach of a new equilibrium state indicated in blue (fast adjustment) and black (equilibrium state) in Fig. 17. Also in this case, the distribution changes are directly visible on the beam profiles taken with the BSRT (see Appendix B, Fig. 30).

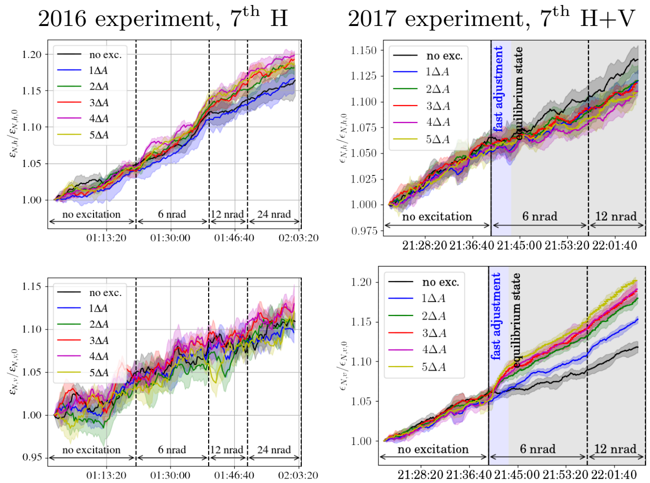

FIG. 17. Relative horizontal (top) and vertical (bottom) emittance obtained during the 2016 experiments (left) and the 2017 experiment (right) averaged over the bunches experiencing the same excitation amplitude. For all bunches the damper was not active.

The loss rates measured during the experiment however differ from the simulations in terms of for which case the largest rate is observed as well as quantitatively for the specific cases. For example smaller losses are expected for the 2016 experiments compared to the 2017 experiments from simulations, while experimentally higher loss rates were measured in 2016 (see Fig. 18). For the 2017 experiment, the highest loss rates are expected for pulsing in H+V, than in H and then with a considerably reduction in V. During the experiment comparable loss rates are however measured for all three planes (see Appendix B, Fig. 29)

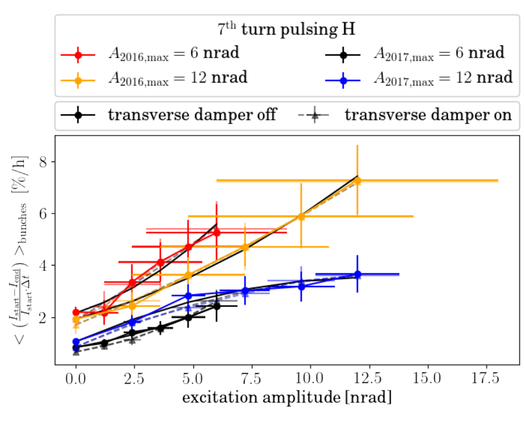

FIG. 18. Comparison of scaling of loss rates with excitation amplitude for 7th turn pulsing in H and data obtained during the 2016 experiment (black and blue) and 2017 experiment (red and yellow). The excitation amplitude error is 50% in 2016 and could be reduced to 15% in 2017.

D. 8th turn pulsing

Pulsing patterns which have little effect on the beam core are particularly interesting for the hollow electron lens operation if they in addition have a large effect on the halo, which is in general feasible considering the highly nonlinear field generated at the location of the halo particles by the HEL. With this motivation in mind the 8th turn pulsing pattern was studied, for which a small effect in comparison to the 7th and 10th turn pulsing is expected from the distribution tracking summarized in Fig. 19.

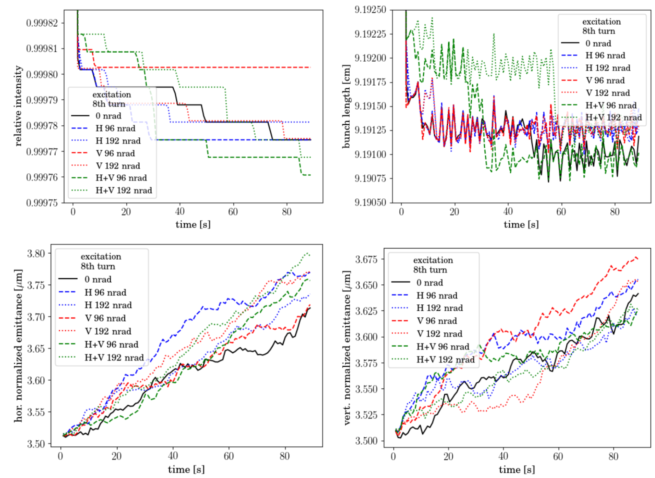

FIG. 19. Relative intensity (top left), bunch length (top right), and horizontal (bottom left) and vertical (bottom right) emittance obtained from simulations (distribution tracking) based on the 2017 injection optics with standard errors and $(Q_x, Q_y) = (62.27, 60.295)$. The solid line indicates an excitation with only a random dipole noise component in H+V of 6 nrad, and the dotted and dashed line the results for 8th turn pulsing plus a random dipole noise component in H+V of 6 nrad.

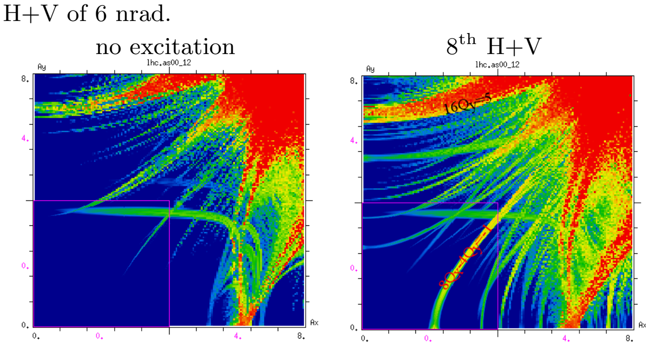

FIG. 20. FMA analysis in amplitude space without excitation (left) and for 8th turn pulsing (right) based on the 2017 injection optics with no machine errors and a tune of (62.27,60.295). The excitation is 96 nrad in both planes. The $16Q_y$ and $8Q_x - 4Q_y$ are both excited.

For excitation amplitudes smaller than 96 nrad no visible effect is indeed observed. In the horizontal and vertical plane a small emittance growth due to the excitation is visible, but without any clear dependency on the amplitude nor plane. Adducting the FMA analysis in amplitude space shown in Fig. 20, the 8^{th} turn pulsing drives the $16Q_y$ and $8Q_x - 4Q_y$ resonances and several even higher orders. These are in general very high order resonances whose effect is thus expected to be small.

The only small effect on the beam expected from simulations could then be also confirmed experimentally during the 2017 experiment. For this purpose the excitation amplitude was increased to 96 nrad, which is the maximum kick strength reachable with the transverse damper at injection without risking saturation. As depicted in Fig. 21, the loss rate increased slightly with the excitation amplitude for an excitation in H+V. For an excitation only in V or only in H, no statistically relevant increase was observed.

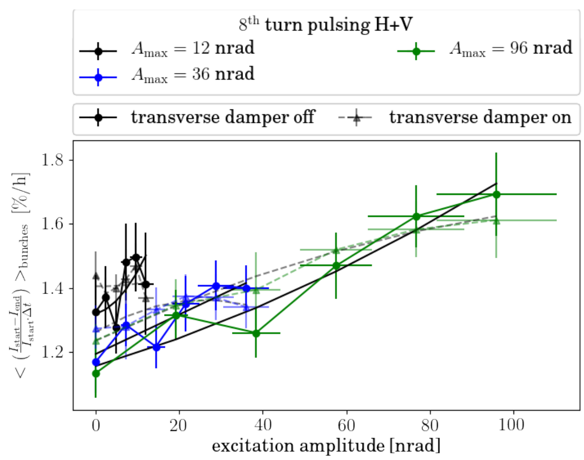

FIG. 21. Comparison of scaling of loss rates with excitation amplitude for 8^{th} turn pulsing in H+V measured during the 2017 experiment. The excitation amplitude error is 15% indicated by the horizontal error bars.

In the horizontal plane, a change in beam distribution was measured with the BSRT profiles (Appendix C, Fig. 31) for an excitation only in H, explicitly an increase of the distribution at around 2.0 σ simultaneously with a depletion of the beam core. For an excitation in H+V the emittances of the references bunches were much smaller, around 1.8 μm normalized emittance on average, than the ones of the excited bunches ranging from 2.3 μm to 3.0 μm as described in [20]. The references bunches thus experienced a stronger emittance growth due to intra-beam scattering than the excited bunches due to the excitation on top of their smaller emittance growth due to intra-beam scattering. Therefore no excitation amplitude dependent emittance growth was observed for an excitation in H+V albeit it was recorded for an excitation only in H. In the vertical plane, the beam distribution and thus emittance stayed unchanged. For an excitation only in V, no dependence on the excitation was measured.

E. random excitation

The random excitation presents in general the pulsing pattern leading to the fastest halo depletion rates achievable with an HEL. On the other hand this pattern is also the most dangerous one for the proton beam core. The aim of this experiment was to test the effect on the core in comparison to the resonant excitation represented in the 2017 experiment by primarily the 7^{th} turn pulsing as for 8^{th} turn pulsing basically no effect was observed. The random excitation is in general so powerful as it excites all frequencies of the beam equally. This can be

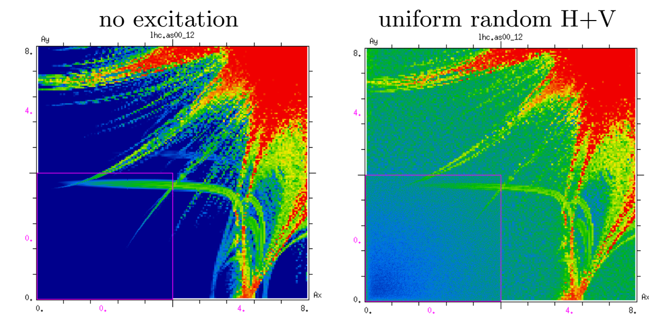

FIG. 22. FMA analysis in amplitude space without excitation (left) and for a uniform random excitation with 1 nrad amplitude (right) in H+V based on the 2017 injection optics with no machine errors and a tune of (62.27,60.295).

seen formidably on the example of the FMA analysis in amplitude space, depicted in Fig. 22, for a random excitation as applied during the 2017 experiment. In this case, the diffusion in tune is increased equally by the random excitation independent of the particle amplitude.

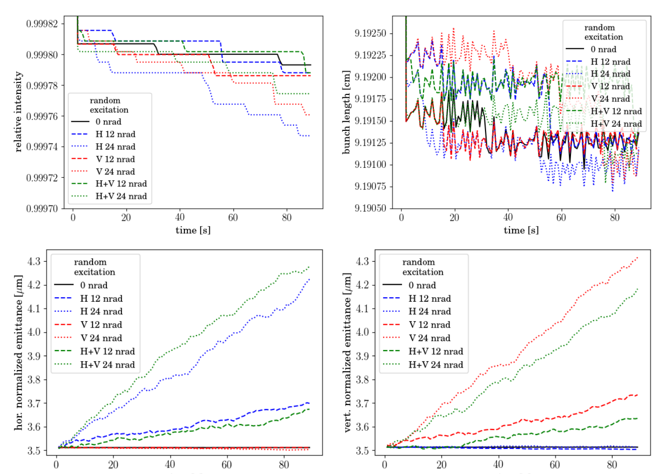

FIG. 23. Relative intensity (top left), bunch length (top right), and horizontal (bottom left) and vertical (bottom right) emittance obtained from distribution tracking based on the 2017 injection optics with standard errors and $(Q_x, Q_y) = (62.27, 60.295)$. The solid line indicates the case with no excitation, and the dotted and dashed line the results for a uniform random excitation of 12 nrad and 24 nrad respectively.

The results from the distribution tracking are shown in Fig. 23. In contrast to the 7^{th} and 10^{th} turn pulsing, the effect of a random excitation is very symmetric:

- Emittance growth is only caused in the plane of excitation.
- The emittance growth is comparable between an excitation in H and V in the corresponding plane as well as the scaling with the excitation amplitude. Only a small increase or decrease is observed if the excitation is applied in both planes. The difference could be due to coupling.
- The random excitation leads to an increased constant emittance growth rate which is reached without undergoing an initial adjustment phase.
- Negligible losses are observed independent of the plane of excitation.

Qualitatively, this behavior could be also confirmed experimentally during the 2017 experiments, where excitation amplitude dependent emittance growth was only recorded in the plane of excitation with all excitation amplitude dependent emittance growth rates in a comparable range. As example the relative horizontal and vertical emittance for pulsing in V and in H+V are depicted in Fig. 24. Note that as expected from simulations and despite the large excitation amplitude dependent emittance growth, the growth rate stays constant and there is explicitly no fast adjustment phase succeeded by a new equilibrium state as was observed for the 7^{th} and 10^{th} turn pulsing.

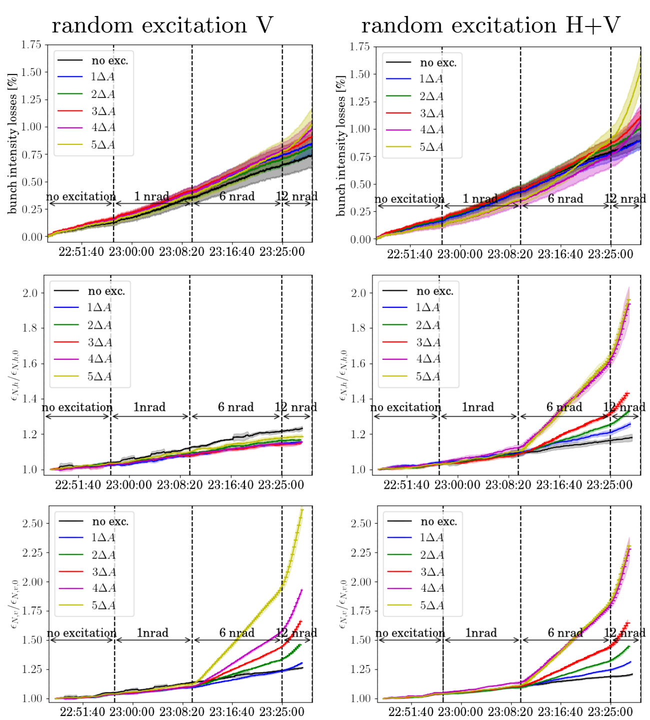

FIG. 24. Relative intensity (top) and relative horizontal (center) and vertical (bottom) emittance for a random excitation only in V (left) and in H+V (right). Emittance growth is only caused in the plane of excitation.

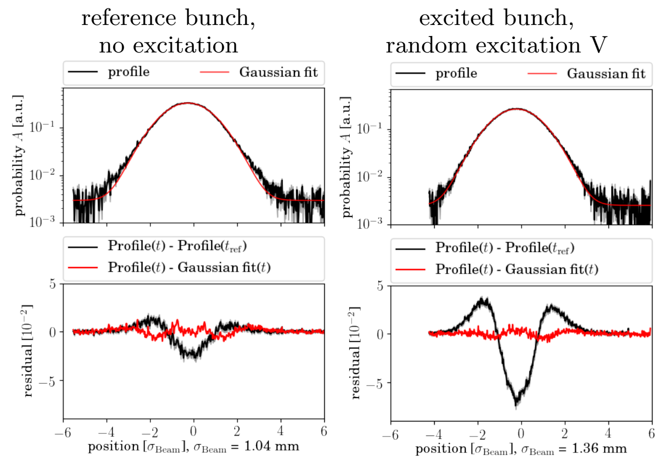

FIG. 25. Vertical beam profiles measured with the Beam Synchrotron Radiation Telescope (BSRT) during the 2017 experiments. The profiles are taken at the end of the random excitation in V. For both bunches the transverse damper is not active. The distribution changes in the reference bunch (left), here slot 1698, are much less than for the bunch experiencing the maximum excitation (right), here slot 2696.

The large changes of the emittance are of course also directly visible in the beam profiles measured with the BSRT shown in Fig. 25 for a random excitation only in V. In comparison to the 10^{th} turn pulsing shown in Fig. 12, the distribution also stays Gaussian in case of a random excitation while for the 10^{th} turn pulsing it clearly adopts to a non-Gaussian shape.

The experimental results for a maximum excitation amplitude of $A_{\max} = 1$ nrad and $A_{\max} = 6$ nrad also confirm the in general small losses predicted in simulations. The losses then suddenly increase once the maximum ex-

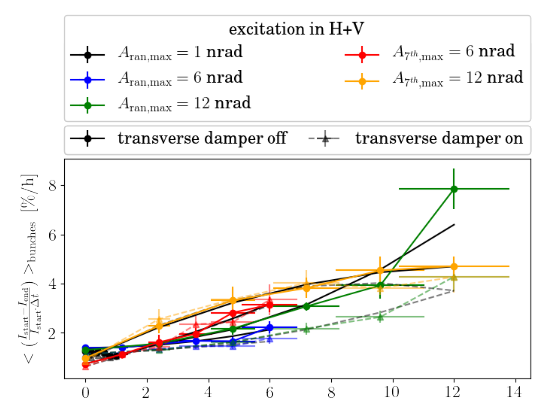

FIG. 26. Comparison of scaling of loss rates with excitation amplitude for a random excitation and 7^{th} turn pulsing in H+V measured during the 2017 experiment. The excitation amplitude error is 15% indicated by the horizontal error bars.

citation amplitude is increased to $A_{\max} = 12$ nrad, which is most likely the point when, due to the large emittance increase, the physical aperture starts eating into the more central region of the distribution resulting in higher losses despite the larger emittance growth for a random excitation. In comparison to the 7^{th} turn pulsing, the loss rate for a random excitation is smaller for a maximum excitation amplitude of $A_{\max} = 6$ nrad, but larger for $A_{\max} = 12$ nrad (see Fig. 26). This indicates an increase of the diffusion mostly in the beam tails for 7^{th} turn pulsing, while for a random excitation mostly the core is affected. Furthermore, the dependence of the loss rate on the excitation plane is additive, meaning that double the loss rate is observed for an excitation in H+V compared to only in H or only V (see Appendix D, Fig. 32). In view of the next section, Sec. V F, not that the loss rate is also considerably reduced for a random excitation if the transverse damper is active, while in case of the 7^{th} turn pulsing the loss rate does not change.

F. Effect of the transverse damper

For all k^{th} turn pulsing patterns, the transverse damper does in general not change any of the observables studied during the experiments, explicitly losses, emittance and beam distribution suggesting that indeed it is not capable of damping any resonant excitation. On the other hand, the transverse damper considerably decreases any changes of the above parameters in case of a random excitation. As an example, the vertical emittance growth for the 7^{th} turn pulsing in V is compared with a random excitation in V in Fig. 27 and the loss rates

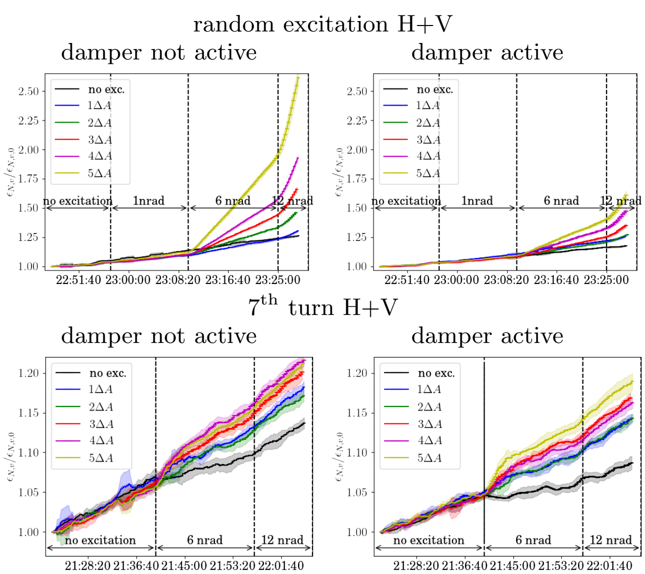

FIG. 27. Relative intensity for bunches with transverse damper not active (top) and transverse damper active (bottom) for 7^{th} turn pulsing in V (left) and for a random excitation only in V (right).

in Fig. 26 illustrating impressively the aforesaid behavior. Any idea why? Daniel, help!

VI. SUMMARY

This paper intends to give an overview of the effects of the HEL on the proton beam core and the experiments conducted in this context at the LHC in 2016 [19] and 2017 [20]. For a perfect HEL without any imperfections no effect on the core is to be expected as the field at the center vanishes by construction. Only in the case of imperfections in the guidance and profile of the electron beam, a residual kick on the proton beam core can occur. In this case and assuming HL-LHC parameters (Tables II–III), the contribution from the electron lens bends with approximately 0.5 nrad to first order is negligible with respect to the kick expected from the central region of the HEL of approximatley 20 nrad to first order caused by profile imperfections in the electron beam.

In DC operation these kicks, even if nonlinear in reality, are negligible compared to the nonlinearities present in the LHC and HL-LHC and are thus of no concern. The picture changes if the HEL is operated in pulsed mode, in which case noise is introduced on the halo particles (intended) as well as on the beam core (unintended) in the presence of imperfections of the HEL entailing much more stringent tolerances.

To study the effect on the beam core in case of the much more dangerous pulsed operation, beam experiments were conducted in 2016 and 2017 at injection. The experimental results in general suggest that for the kick amplitudes as expected from the HEL, considerable effects are to be expected for a random excitation and certain resonant excitations, explicitly 7^{th} and 10^{th} turn pulsing during the conducted experiments. In addition, also one resonant excitation pattern, the 8^{th} turn pulsing, was tested featuring a small effect on the beam core. Assuming that this pattern has a large effect on the beam halo, it would be an optimal candidate for a feasible HEL excitation pattern.

The resonant excitation in general features a rich nonlinear dynamics leading to a diversity in beam distribution and diffusion changes as can be seen for example from the very diverse effects of the different k^{th} turn pulsing patterns observed in simulations and experiments. The origin of this diversity is due to the fact that only certain frequencies and thus resonances are excited. Typical for the resonant excitation is also the fast adjustment of the beam distribution to a new equilibrium state which could be for the first time measured in the experiments and predicted in the simulations presented in this paper. The random excitation on the other hand excites all beam frequencies equally, leading to the highest increase in halo removal rates for the HEL [13] but also the strongest effects on the core, mainly in terms of strong emittance growth as predicted in simulations, experiments and also a multitude of earlier publications on the subject of random noise.

In summary, the effects of the HEL on the beam core in case of pulsed operation are not negligible. Tolerances in case of a random excitation are extremely stringent, while a resonant excitation appears feasible if the order k of the k^{th} turn pulsing is tuned to the machine and beam configuration, explicitly tune, tune spread and machine nonlinearities.

ACKNOWLEDGMENTS

We wish to acknowledge Giulia Papotti with her help with the preparations for the 2016 experiments and her general support from the operations side, Roderik Bruce and Gianluca Valentino for there very helpful suggestions in preparing the experiment at the LHC and we would like to thank all participants of the experiment for helping acquire the data presented in this paper. We would like to acknowledge Dmitry Shatilov for his help with the Lifetrac code, and Stéphane Fartoukh, Riccardo De Maria and Rogelio Toms for their help with generating the appropiate optics model. We are grateful also for the support from the beam instrumentation team, in particular Enrico Bravin and Georges Trad, with the BSRT and are thankful for the collaboration with Stéphania Papadopoulou and Fanouria Antonio for the analysis of the BSRT profiles.

Appendix A: Additional plots for 10th turn pulsing during the 2016 experiments

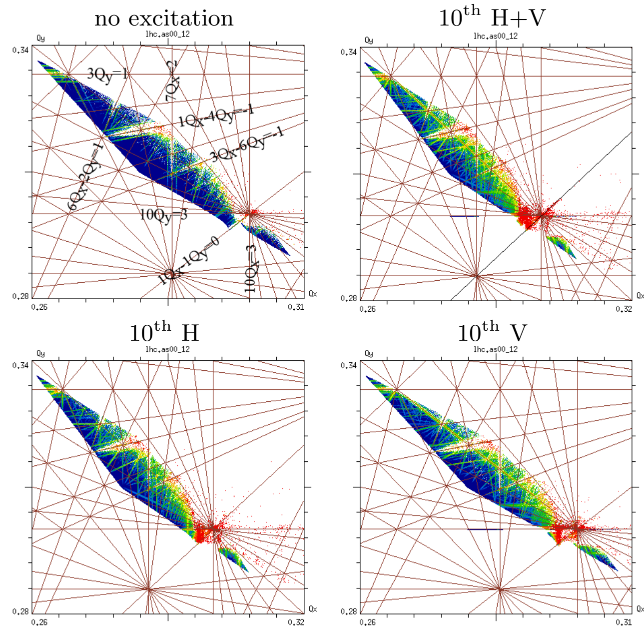

FIG. 28. FMA analysis for 10^{th} turn pulsing based on the 2016 injection optics with no machine errors and a tune of (64.28,59.31). The excitation is 120 nrad in the corresponding plane. There is no significant difference in the FMA analysis between pulsing only in H, only in V or in H+V.

Appendix B: Additional plots for 7^{th} turn pulsing during 2017 experiments

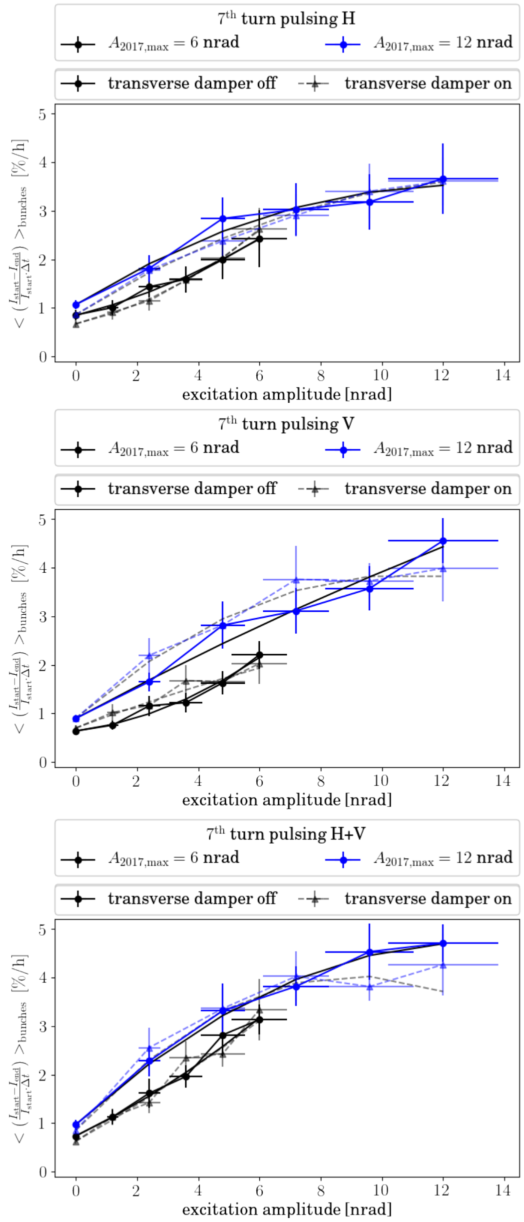

FIG. 29. Comparison of scaling of loss rates with excitation amplitude for 7^{th} turn pulsing in only in H (top), only in V (top) and in H+V during the 2017 experiment. The excitation amplitude error is 15% indicated by horizontal error bars. The vertical errorbars represent the pure statistical error based on the averaging over several bunches with the same excitation amplitude.

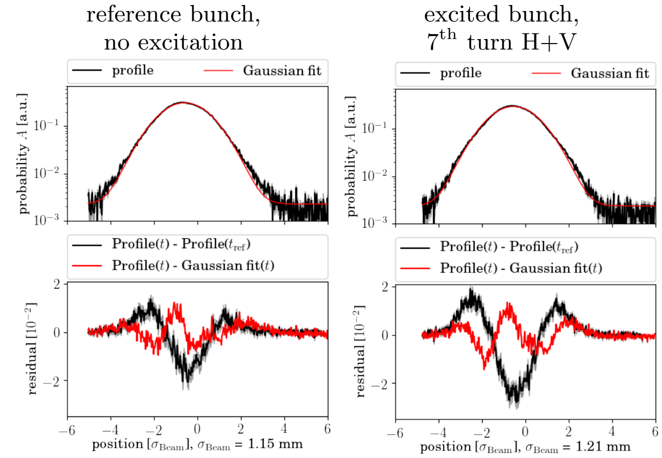

FIG. 30. Vertical beam profiles measured with the Beam Synchrotron Radiation Telescope (BSRT) during the 2017 experiments. The profiles are taken at the end of the 7^{th} turn pulsing in H+V. For both bunches the transverse damper is not active. The distribution changes in the reference bunch (left), here slot 2862, are much less than for the bunch experiencing the maximum excitation (right), here slot 2696.

Appendix C: Additional plots for 8^{th} turn pulsing during 2017 experiments

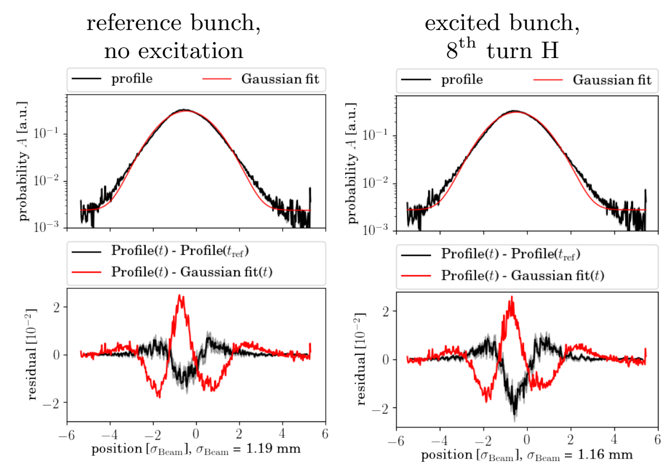

FIG. 31. Horizontal beam profiles measured with the Beam Synchrotron Radiation Telescope (BSRT) during the 2017 experiments. The profiles are taken at the end of the 8^{th} turn pulsing in H. For both bunches the transverse damper is not active. The distribution changes in the reference bunch (left), here slot 804, are much less than for the bunch experiencing the maximum excitation (right), here slot 632.

Appendix D: Additional plots for random excitation during 2017 experiments

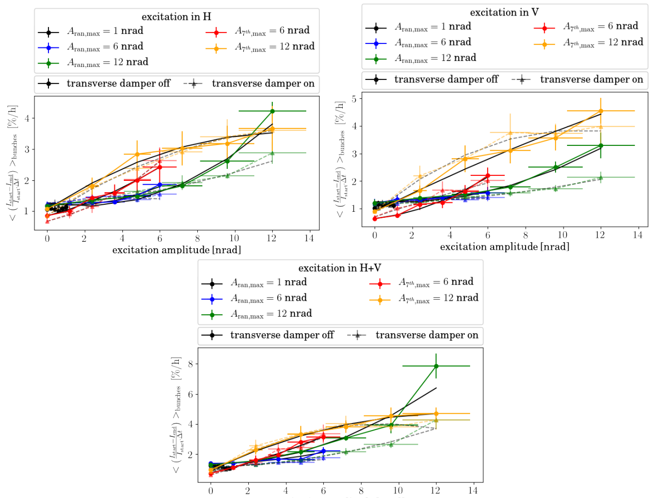

FIG. 32. Comparison of scaling of loss rates with excitation amplitude for a random excitation and 7$^{\mathrm{th}}$ turn pulsing only in H (top), only in V (center) and in H+V (bottom) measured during the 2017 experiment. The excitation amplitude error is 15% indicated by the horizontal error bars. Note that for 7$^{\mathrm{th}}$ turn pulsing the transverse damper does not influence the loss rate, while for a random excitation the loss rate is considerably reduced for the bunches with transverse damper active.

[1] S. Holmes, R. S. Moore, and V. Shiltsev, Journal of Instrumentation **6**, T08001 (2011).

[2] D. Nisbet, "2016 operation: Operational efficiency and lessons learnt," (2017), LHC Performance Workshop 2017.

[3] O. S. Brüning, P. Collier, P. Lebrun, S. Myers, R. Ostojic, J. Poole, and P. Proudlock, *LHC Design Report*, CERN Yellow Reports: Monographs (CERN, Geneva, 2004).

[4] A. G., B. A. I., B. O., F. P., L. M., R. L., and T. L., *High-Luminosity Large Hadron Collider (HL-LHC): Technical Design Report V. 0.1*, CERN Yellow Reports: Monographs (CERN, Geneva, 2017).

[5] M. Benedikt and F. Zimmermann, *Future Circular Colliders*, Tech. Rep. CERN-ACC-2015-0164 (CERN, Geneva, 2015).

[6] G. Valentino, "What did we learn about halo population during MDs and regular operation?" (2016), Review of the needs for a hollow e-lens for the HL-LHC.

[7] "Review on the needs for a hollow e-lens for the HL-LHC," (2016).

[8] *Proceedings, EuCARD-AccNet-EuroLumi Workshop: The High-Energy Large Hadron Collider (HE-LHC10): Villa Bighi, Malta, Republic of Malta, October 14-16, 2010* (2011) arXiv:1108.1617 [physics.acc-ph].

[9] J. Molson, R. Bruce, A. Faus-Golfe, M. Fiascaris, A. Krainer, and S. Redaelli, in *Proceedings, 8th International Particle Accelerator Conference (IPAC 2017): Copenhagen, Denmark, May 14-19, 2017* (2017) p. MOPAB001.

[10] R. Bruce, "Alternative methods for halo depletion (damper, tune modulation, and wire), long range beam-beam and comparison of their performance/reliability to that of a hollow electron lens." (2016), review of the needs for a hollow e-lens for the HL-LHC.

[11] "Hl-lhc optics v1.3," LHC optics web.

[12] G. Stancari, V. Previtali, A. Valishev, R. Bruce, S. Redaelli, A. Rossi, and B. S. Ferrando, *Conceptual design of hollow electron lenses for beam halo control in the Large Hadron Collider*, Tech. Rep. FERMILAB-TM-2572-APC, CERN-ACC-2014-0248 (Fermilab, CERN, 2014) arXiv:1405.2033 [physics.acc-ph].

[13] M. Fitterer, G. Stancari, and A. Valishev, *Simulation Study of Hollow Electron Beam Collimation in HL-LHC*, Tech. Rep. FERMILAB-TM-2636-AD (Fermilab, 2016).

[14] M. Fitterer, G. Stancari, a. Valishev, R. De Maria, S. Redaelli, K. Sjobak, and J. F. Wagner, in *Proceedings, 8th International Particle Accelerator Conference (IPAC 2017): Copenhagen, Denmark, May 14-19, 2017* (2017) p. THPAB041.

[15] M. Fitterer, G. Stancari, and A. Valishev, *Effect of pulsed hollow electron-lens operation on the proton beam core in LHC*, Tech. Rep. FERMILAB-TM-2635-AD (Fermilab, 2016).

[16] X.-L. Zhang, K. Bishofberger, V. Kamerdzhiev, V. Lebedev, V. Shiltsev, R. Thurman-Keup, and A. Tollestrup, Phys. Rev. ST Accel. Beams **11**, 051002 (2008).

[17] G. Stancari, *Calculation of the Transverse Kicks Generated by the Bends of a Hollow Electron Lens*, Tech. Rep. FERMILAB-FN-0972-APC (Fermilab, 2014) arXiv:1403.6370 [physics.acc-ph].

[18] I. A. Morozov, G. Stancari, A. Valishev, and D. N. Shatilov, *Proceedings, 3rd International Conference on Particle accelerator (IPAC 2012): New Orleans, USA, May 2-25, 2012*, Conf. Proc. IPAC 2012 **C1205201**, 94 (2012).

[19] M. Fitterer, G. Stancari, A. Valishev, R. Bruce, P. S. Papadopoulou, G. Papotti, D. Pellegrini, S. Redaelli, G. Trad, D. Valuch, G. Valentino, J. Wagner, and C. Xu, (2016).

[20] M. Fitterer, G. Stancari, A. Valishev, R. Bruce, P. S. Papadopoulou, G. Papotti, D. Pellegrini, S. Redaelli, G. Trad, D. Valuch, G. Valentino, J. Wagner, and C. Xu, (2018).

[21] "Electron lens test stand,".

[22] G. Stancari, "Electron-beam simulations: electron-gun emission and residual fields from measured profiles," HEL Electron Beam results discussion.

[23] "The warp code,".

[24] M. Fitterer and G. Stancari, *Analysis of BSRT profiles in the LHC at injection*, Tech. Rep. FERMILAB-TM-2657-AD-APC (Fermilab, 2017).

[25] T. Linnecar, M. E. Angoletta, L. Arnaudon, P. Baudrenghien, T. Bohl, O. Brunner, A. Butterworth, E. Ciapala, F. Dubouchet, J. Ferreira-Bento, D. Glenat, G. Hagmann, W. Hfle, C. Julie, F. Killing, G. Kotzian, D. Landre, R. Louwerse, P. Maesen, P. Martinez-Yanez, J. Molendijk, E. Montesinos, C. Nicou, J. Noirjean, G. Papotti, A. Pashnin, G. Pechaud, J. Pradier, V. Rossi, J. Sanchez-Quesada, M. Schokker, E. Shaposhnikova, R. Sorokoletev, D. Stellfeld, J. Tckmantel, D. Valuch, U. Wehrle, and F. Weierud, *Hardware and Initial Beam Commissioning of the LHC RF Systems*, Tech. Rep. LHC-PROJECT-Report-1172. CERN-LHC-PROJECT-Report-1172 (CERN, Geneva, 2008).

[26] W. Höfle, G. Kotzian, M. Schokker, and D. Valuch, "LHC Damper Beam commissioning in 2010," (2011).

[27] X. Buffat, J. Barranco Garca, T. Pieloni, C. Tambasco, and D. Valuch, Conf. Proc. IPAC 2017 (2017).

[28] J. Laskar, *Particle accelerator. Proceedings, Conference, PAC 2003, Portland, USA, May 12-16, 2003*, Conf. Proc. **C030512**, 378 (2003).

[29] D. Shatilov, Y. Alexahin, V. Lebedev, and A. Valishev, *Particle accelerator. Proceedings, Conference, PAC'05,Knoxville, USA, May 16-20, 2005*, Conf. Proc. PAC'05 (2005).

[30] X. Buffat, N. Biancacci, S. V. Furuseth, D. Jacquet, E. Metral, D. Pellegrini, M. Pojer, G. Trad, D. Valuch, J. Barranco Garcia, T. Pieloni, C. Tambasco, and Q. Li, (2017).

[31] J. Barranco Garcia, X. Buffat, T. Pieloni, C. Tambasco, G. Trad, D. Valuch, M. Betz, M. Wendt, M. Pojer, M. Solfaroli Camillocci, B. M. Salvachua Ferrando, K. Fuchsberger, M. Albert, and J. Qiang, *MD 400: LHC emittance growth in presence of an external source of noise during collision*, Tech. Rep. CERN-ACC-NOTE-2016-0020 (CERN, 2016).